MOLECULAR AND CELLULAR BIOLOGY, Apr. 1999, p. 3103–3114 Vol. 19, No. 4
0270-7306/99/$04.00+0

Control of Replicative Life Span in Human Cells: Barriers to Clonal Expansion Intermediate Between M1 Senescence and M2 Crisis

J. A. BOND, M. F. HAUGHTON, J. M. ROWSON, P. J. SMITH, V. GIRE, D. WYNFORD-THOMAS,* AND F. S. WYLLIE

Cancer Research Campaign Laboratories, Department of Pathology, University of Wales College of Medicine, Heath Park, Cardiff CF4 4XN, United Kingdom

Received 28 August 1998/Returned for modification 16 October 1998/Accepted 11 January 1999

The accumulation of genetic abnormalities in a developing tumor is driven, at least in part, by the need to overcome inherent restraints on the replicative life span of human cells, two of which—senescence (M1) and crisis (M2)—have been well characterized. Here we describe additional barriers to clonal expansion (M^{int}) intermediate between M1 and M2, revealed by abrogation of tumor-suppressor gene (TSG) pathways by individual human papillomavirus type 16 (HPV16) proteins. In human fibroblasts, abrogation of p53 function by HPVE6 allowed escape from M1, followed up to 20 population doublings (PD) later by a second viable proliferation arrest state, $M^{int}E6$, closely resembling M1. This occurred despite abrogation of $p21^{WAF1}$ induction but was associated with and potentially mediated by a further ~3-fold increase in $p16^{INK4a}$ expression compared to its level at M1. Expression of HPVE7, which targets pRb (and $p21^{WAF1}$), also permitted clonal expansion, but this was limited predominantly by increasing cell death, resulting in a $M^{int}E7$ phenotype similar to M2 but occurring after fewer PD. This was associated with, and at least partly due to, an increase in nuclear p53 content and activity, not seen in younger cells expressing E7. In a different cell type, thyroid epithelium, E7 also allowed clonal expansion terminating in a similar state to $M^{int}E7$ in fibroblasts. In contrast, however, there was no evidence for a p53-regulated pathway; E6 was without effect, and the increases in $p21^{WAF1}$ expression at M1 and $M^{int}E7$ were p53 independent. These data provide a model for clonal evolution by successive TSG inactivation and suggest that cell type diversity in life span regulation may determine the pattern of gene mutation in the corresponding tumors.

Human tumors develop by a process of clonal evolution mediated by the acquisition of successive molecular abnormalities and driven, at least in part, by the need to overcome the inherent controls which limit the proliferative life span of normal human cells (51).

Two of these proliferative life span barriers (PLBs)—senescence and crisis—have been well characterized, particularly with respect to human fibroblast models. These cells normally undergo around 40 to 70 population doublings (PD) (depending on age of donor) after which, even in ideal culture conditions, they enter a stable proliferative arrest in which they remain viable for many months (27). Escape from this state of replicative senescence, or mortality stage 1 (M1) (48), can be conferred by expression of a variety of DNA tumor virus genes, including simian virus 40 (SV40) T and human papillomavirus type 16 (HPV16) E6 plus E7, which target a common set of cell cycle regulatory tumor suppressor gene products, notably p53 and pRb (14, 41). The resulting clones are capable of at least an additional 30 PD, after which further expansion is limited by a second PLB termed crisis (or M2), which is due not so much to decreasing proliferation as to increasing cell death. Escape from this state is associated with stabilization of telomere length by reactivation of telomerase or equivalent mechanisms (4, 15).

In naturally-occurring tumors unrelated to viral pathogenesis, multiple independent mutational events are of course required to achieve the same effect as a single multifunctional viral agent. On the assumption that, for at least a subset of these mutations, the selection pressure is an extension of proliferative life span, it can be predicted that instead of a single M1, there should be multiple PLBs which need to be bypassed by loss of successive cell cycle inhibitors before M2 can be reached.

This prediction is supported by the frequent finding that loss of individual tumor suppressor pathways, achieved by expression of a subset of viral functions (e.g., HPV E6 or E7 or SV40 T domain mutants), while allowing escape from M1, appears to confer a more limited extension of life span than that obtained with the full combination (41). This has also been demonstrated with respect to p53 by using a dominant-negative approach (11) and by observing the results of spontaneous loss of wild-type (wt) p53 in a strain of Li-Fraumeni syndrome (LFS) fibroblasts (39). The latter revealed a clear intermediate state of growth arrest between M1 and M2, from which cells could escape if the Rb pathway is also compromised, for example, by loss of $p16^{INK4a}$ expression.

Despite their obvious significance for human tumor progression, these intermediate PLBs have not been studied in the detail devoted to the classic M1 and M2 states. Indeed, their very existence is sometimes ignored. In particular, the life span of human fibroblasts expressing HPVE6 has been assumed to end in a state identical to "normal" M1 senescence (34, 42), leading to potential misinterpretations, including the conclusion that p21 is not essential for senescence.

The aims of this work therefore were (i) to characterize in detail the phenotype of these intermediate PLBs (referred to here as M^{int} by extension of the M1 and M2 terminology), initially by using the human fibroblast paradigm; (ii) to begin to analyze their underlying mechanisms; and (iii) to investigate

* Corresponding author. Mailing address: Cancer Research Campaign Laboratories, Department of Pathology, University of Wales College of Medicine, Heath Park, Cardiff CF4 4XN, United Kingdom. Phone: 44 (0)1222 742700. Fax: 44 (0)1222 743524. E-mail: KingTD@Cardiff.ac.uk.

the extent to which they show diversity between different cell lineages.

MATERIALS AND METHODS

Cells and culture conditions. Normal human diploid fibroblasts (HDF) (HCA2 cells, kindly provided by James Smith, Houston, Tex.) were grown in Dulbecco's modified Eagle medium (DMEM) (Life Technologies, Paisley, United Kingdom) supplemented with 10% fetal calf serum (FCS) (Imperial Labs, London, United Kingdom). Determination of in vitro life span and passage protocols were as described in reference 10. Senescence, as defined by the criteria described previously (23), occurred at an estimated population doubling level (PDL) of 66 to 67.

Primary monolayer cultures of follicular epithelial cells were prepared from surgical samples of normal human thyroid tissue by protease digestion and mechanical disaggregation (46). Cells were grown as monolayers in a 2:1:1 mixture of DMEM, Ham's F12, and MCDB104 (all from Life Technologies) (7), supplemented with 10% FCS.

Retroviral gene transfer. Amphotropic retrovirus vectors expressing HPV16E6 and/or E7 genes from a pLXSN construct, packaged in PA317 cells (25), were kindly provided by Denise Galloway, Seattle, Wash. As a neo-only control, a pBABEneo vector, packaged in ψ-CRIP cells, was used (49). The initial titers as assessed by transduction of G418 resistance to a human cell line (A431) were 1×10^6, 1.4×10^6, and 2×10^5 CFU/ml for E6, E7, and neo only, respectively, and were equalized by dilution of supernatants prior to use.

Gene transfer was carried out as described previously for fibroblasts (11) and thyroid cells (9). Two days later, fibroblast cultures were passaged into G418 selection (0.4 mg/ml) at a split ratio of 1:4 and observed for colony development. For thyroid cultures, G418 selection was not applied until epithelial colonies became well established, because earlier use gives a diminished yield and is not necessary, given the very limited proliferative life span of uninfected thyroid epithelial cells.

BrdU incorporation. Cells were labelled by incubation in 10 μM bromodeoxyuridine (BrdU) for 1 h, following which BrdU incorporation was detected as previously described by immunoperoxidase (8) or immunofluorescence (23) methods, except that, for the latter, a rat anti-BrdU antibody (Sera Labs) was used.

Detection of SAβ-gal activity. Endogenous senescence-associated mammalian β-galactosidase activity (SAβ-gal) (19) was assessed histochemically. Cells on coverslips were fixed in 0.5% glutaraldehyde (in phosphate-buffered saline [PBS]) for 15 min and then permeabilized with 0.02% Nonidet P-40 (NP-40)–0.1% sodium deoxycholate for 15 min. This procedure was followed by incubation (overnight at 37°C) in a 1-mg/ml solution of X-Gal substrate (5-bromo-4-chloro-3-indolyl-β-D-galactopyranoside) with 5 mM potassium ferricyanide, 5 mM potassium ferrocyanide, and 2 mM magnesium chloride, together with the above-mentioned detergents, at an acidic pH (6.0). After counterstaining with hematoxylin, the proportion of β-galactosidase (β-Gal)-positive cells was assessed in a total count of >500 cells.

TdT assay. Cytospin preparations of trypsinized cultures were fixed with 4% paraformaldehyde (30 min). Endogenous peroxidase was blocked with 0.3% H_2O_2 in methanol (30 min), and the cells were permeabilized with 0.1% Triton X-100 in 0.1% sodium citrate (15 min). This was followed by incubation for 1 h at 37°C with 250 U of terminal deoxynucleotidyl transferase (TdT; Promega, Southampton, United Kingdom) per ml and 1 nmol of biotin-16-dUTP (Boehringer Mannheim, Lewes, United Kingdom). Sites of biotin-16-dUTP localization were visualized by using the mouse-specific avidin-biotin-peroxidase (ABC) system (Novocastra, Newcastle-upon-Tyne, United Kingdom), followed by incubation in diaminobenzidine-hydrogen peroxide solution. After hematoxylin counterstaining, the proportion of apoptotic (brown) cells was assessed in samples of >1,000 cells.

Immunocytochemistry. For both p53 and $p16^{INK4a}$, monolayers were fixed in acetone-methanol, 1:1 (10 min at −20°C), and a standard indirect immunoperoxidase procedure was applied by using mouse monoclonal antibodies PAb421 (26) and DCS-50 (32) (Ab-1; Calbiochem), respectively, followed by peroxidase-conjugated rabbit anti-mouse immunoglobulin (Ig) (Dako).

For $p21^{WAF1}$, cultures were fixed in 4% paraformaldehyde (10 min) and then pretreated with 100 mM glycine (10 min), 0.2% Triton X-100 (20 min), and 0.3% H_2O_2 (3 min), and nonspecific binding was blocked with 2% horse serum (30 min). Anti-p21 mouse monoclonal antibody (clone 6B6; Cambridge Bioscience [10]) was applied, followed by the mouse-specific avidin-biotin-peroxidase system (Novocastra).

For HPVE7, cultures were fixed in 4% paraformaldehyde (10 min), followed by 50 mM glycine (10 min), 0.2% Triton X-100 (2 min), and 0.3% H_2O_2 (3 min), and nonspecific binding was blocked with 2% horse serum (10 min). Anti-HPV16 E7 monoclonal antibody (product no. 100201; Ciba Corning, Alameda, Calif.) was applied for 45 min, followed by the ABC detection system.

For all four antigens, sites of antibody binding were visualized by the deposition of brown polymer, following incubation in diaminobenzidine-hydrogen peroxide solution.

Immunoblotting. Cells were lysed for 5 min at 4°C by 1% NP-40 in 150 mM NaCl–50 mM Tris (pH 8.0)–5 mM EDTA buffer, containing 1 mM phenylmethylsulfonyl fluoride, 0.01 mg of aprotinin/ml, and 0.01 mg of ml leupeptin/ml. Protein samples (30 μg each) were separated on sodium dodecyl sulfate–12% polyacrylamide gel electrophoresis gels and electroblotted to Transblot polyvinylidene difluoride membrane (Bio-Rad). Anti-p21 and -p16 antibodies (as above) were applied, followed in both cases by goat anti-mouse Ig-peroxidase conjugate and visualization by the enhanced chemiluminescence detection system (Amersham, Little Chalfont, United Kingdom). The filter was stained with India ink, and quantitation of the specific signal and the amount of protein loaded was performed by using a Bio-Rad imaging densitometer with Molecular Analyst software.

Microinjection. Microinjections were performed as described previously (23). Affinity-purified mouse monoclonal anti-p53 antibody PAb1801 (5) (Ab2; Oncogene Science), DO-1 (44) (Ab 6; Oncogene Science), or control mouse IgG (Sigma) was injected at 2 mg/ml. All antibodies were prepared similarly by resuspension of lyophilized preparations in PBS (pH 7.2) and injected into the nuclei of target cells.

Immunofluorescence analysis of microinjected cells. Monolayers were fixed and pretreated as described above for detection of p21. Samples were then incubated for 1 h with a 1:500 dilution (in PBS-bovine serum albumin [BSA]) of rabbit polyclonal anti-p21 antibody (Santa Cruz Biotechnology) followed by rhodamine-conjugated goat anti-rabbit IgG (Southern Biotechnology) at 1:100 in PBS-BSA for 1 h. Fluorescein isothiocyanate-conjugated goat anti-mouse IgG (Southern Biotechnology) was also added simultaneously to detect microinjected mouse antibodies and hence to permit independent identification of microinjected cells. Dishes were mounted in Fluoromount G (Southern Biotechnology) and viewed with an Olympus MT-2 fluorescence microscope. Results are expressed as means ± standard errors of at least three independent experiments, each involving 100 to 200 microinjected cells.

Flow cytometry. After trypsinization and permeabilization, cells were stained with ethidium bromide and treated with ribonuclease, and DNA content was analyzed on a Becton Dickinson FACS Vantage flow cytometer. Forward light scatter was used as the master trigger, and cell doublets were excluded by pulse analysis.

RESULTS

Phenotypes of M^{int} in human fibroblasts expressing HPVE6 or E7. The HCA2 strain of normal diploid fibroblasts was grown to a point very close to senescence (PDL 64/65) before being infected with amphotropic retroviral vectors encoding a neomycin resistance gene alone (49) or together with HPV16 E6, E7, or E6 plus E7 (25). Analysis of G418-resistant populations (designated HCA2.neo, HCA2.E6, HCA2.E7, and HCA2.E6/E7, respectively) was begun 2 to 3 weeks after infection.

As expected (10, 11), cells expressing neo alone ceased proliferating over the first 2 weeks after an average 2 to 3 PD and entered senescence as shown by their characteristic morphology (Fig. 1A), high SAβ-gal index (>90%), very low (<3%) BrdU labelling index (LI), and very low death rate as determined by TdT assay (Fig. 2). Conversely, expression of HPVE6 plus E7 resulted in evasion of senescence and generated very rapidly growing colonies. These were initially similar in morphology to young HCA2 cells, apart from being smaller and less elongated, as noted previously (45), and showed a similar high BrdU LI (49 to 53%) and low SAβ-gal index (2 to 3%). Pooled HCA2.E6/E7 colonies continued to proliferate for 90 to 100 days, after which net growth ceased in a typical crisis (M2) state (41) (Fig. 1D), characterized by continuing mitotic activity (with many bizarre mitoses), a moderately high BrdU LI (10 to 12%), and a coexisting high apoptotic rate (Fig. 2). The majority (>90%) of cells were also SAβ-gal positive (Fig. 2).

Fibroblasts expressing HPVE6 arrest in a state, $M^{int}E6$, which closely resembles M1 senescence. Introduction of HPVE6 resulted initially in rapidly growing colonies with a BrdU LI of 30 to 35% and a much reduced SAβ-gal index (6 to 14%). Growth slowed, however, after approximately 6 weeks and eventually stopped by 10 to 12 weeks after the start of G418 selection (Fig. 3), in a state (referred to here as $M^{int}E6$), in which the cultures could be maintained with occasional refeeding for prolonged periods without any cell loss or gain. As in M1, the arrested cells were large and flattened, with a charac-

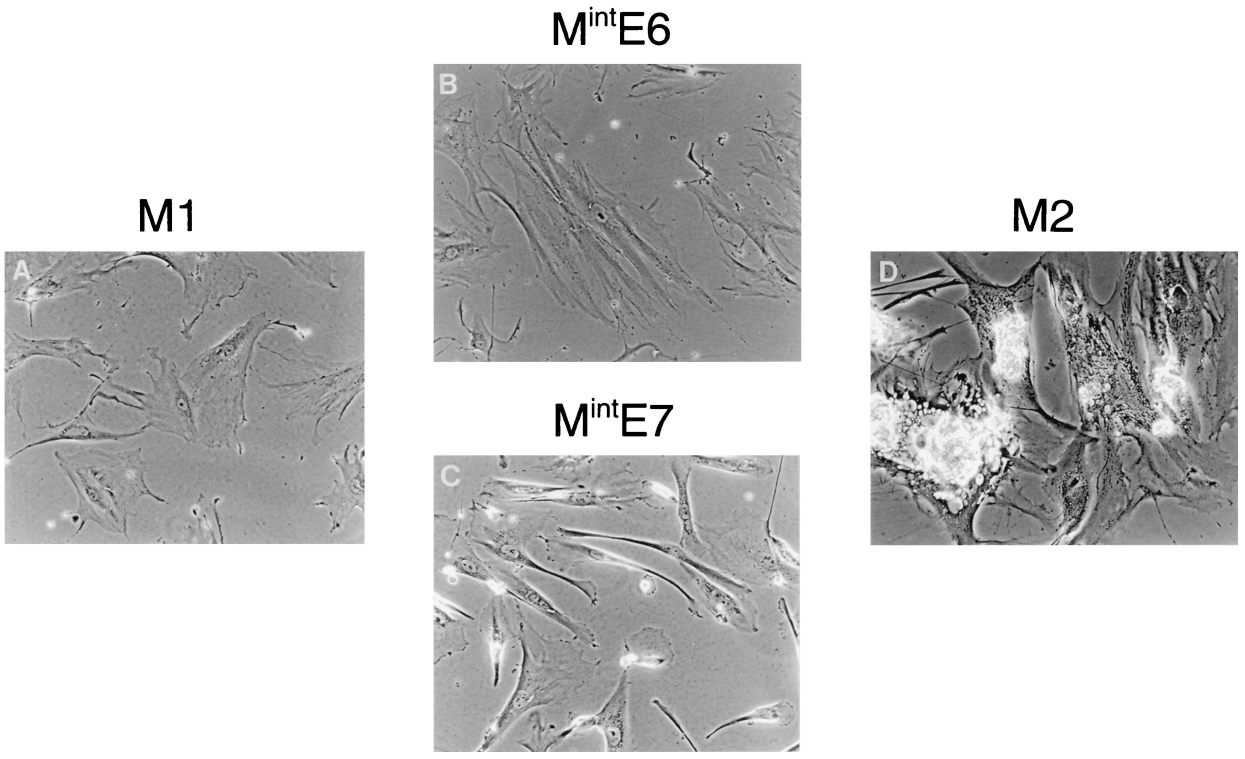

FIG. 1. Comparison of M^{int} phenotypes with M1 (senescence) and M2 (crisis) in HDF. Near-senescent cultures of HDF were infected with retroviral vectors expressing neo only (control) (A), HPVE6 (B), HPVE7 (C), or HPVE6 plus E7 (D) and passaged until they entered a state of zero net growth, designated respectively M1, M^{int}E6, M^{int}E7, and M2. Phase-contrast photomicrographs of M^{int}E6 cultures (B) show cell flattening with very few mitoses or dying cells, a phenotype closely resembling M1 (A). In contrast, M^{int}E7 (C) shows continuing cell turnover resembling M2 (D). Magnification, ×100.

teristic granular cytoplasm (Fig. 1B) and a very high SAβ-gal index (>95%). Again resembling M1, mitoses were rare, the BrdU LI was very low (<2%; Table 1), and apoptotic cells (as defined by nuclear morphology and TdT positivity) were also rare, although not totally absent (Fig. 2). Flow cytometric analysis (data not shown) showed that, as in M1, the majority of cells growth arrested with a 2N DNA content; however, a significant proportion (~20%) had higher levels, reflecting G_2 arrest and/or tetraploidy, and consistent with the appearance of larger and/or more pleomorphic nuclei on phase-contrast examination.

Since it was impossible to know how many population doublings were achieved by the pooled colonies during the initial 2 weeks before G418 selection was complete, individual clones expressing the HPV oncogenes were also selected and expanded. Of 16 clones expressing HPVE6, all ceased proliferating (doubling time > 3 weeks) after periods of up to 8 weeks, again with very few observable mitotic or apoptotic cells. Five clones growth arrested with no more than 10^3 cells, whereas the remaining 11 progressed further up to a maximum cell number of 10^6. Since there was no evidence of cell death at any time, the life span extension conferred by E6 can be estimated from these colony sizes as 10 to 20 PD.

M^{int} in fibroblasts expressing E7 more closely resembles M2 than M1. Introduction of HPVE7 also resulted in rapidly growing colonies with a BrdU LI of 20 to 30%, and an SAβ-gal index which was decreased (49 to 63%), although less so than for E6. HCA2.E7 cultures reached the point of no net growth, termed here M^{int}E7, only 3 to 5 weeks after the start of G418 selection and then entered a phase in which cell death exceeded cell birth, at a time when parallel cultures expressing E6 plus E7 were still undergoing exponential growth with little or no cell death. In most cases, no cells remained by 8 weeks after initial selection (Fig. 3). The difference in kinetics from M^{int}E6 was highlighted by the observation that when HCA2.E7 cultures initially reached the point of no further net growth, their BrdU LI (14 to 22%) was no lower than that seen during the period of initial clonal expansion, although the LI did decrease subsequently. TdT assay provided evidence that cell death at M^{int}E7 was at least partly apoptotic (Fig. 2) and showed that the apoptotic rate increased markedly as the culture approached M^{int}. Despite these resemblances to M2 cultures, however, some M^{int}E7 cells displayed the large, flattened appearance characteristic of M1 or M^{int}E6 fibroblasts (Fig. 1). Flow cytometry (Fig. 4) revealed a marked shift to >2N DNA content compared to both M1 and M^{int}E6 cells, with ~30% in the 4N range and ~5% in the >4N range. There was also a large sub-2N peak indicative of apoptotic fragments, consistent with the TdT data.

Twenty-two individual clones expressing HPVE7 were selected; all showed no net growth after 4 to 6 weeks, with evidence of continuing cell turnover. Twenty failed to exceed 10^3 cells, while two progressed to a maximum of 6×10^3 cells. In the absence of cell loss, this would correspond to an extension of life span of 10 to 13 PD, but given the extensive cell death leading up to M^{int}E7, these must be considered as a significant underestimate of the number of PD attained by some cells.

To allow comparison with M2, five clones expressing both HPVE6 and E7 were also selected. These did not cease proliferation until 12 to 15 weeks after the start of G418 selection when the projected cell number (if no cells had been discarded) would have reached a mean of 2×10^9 with a maxi-

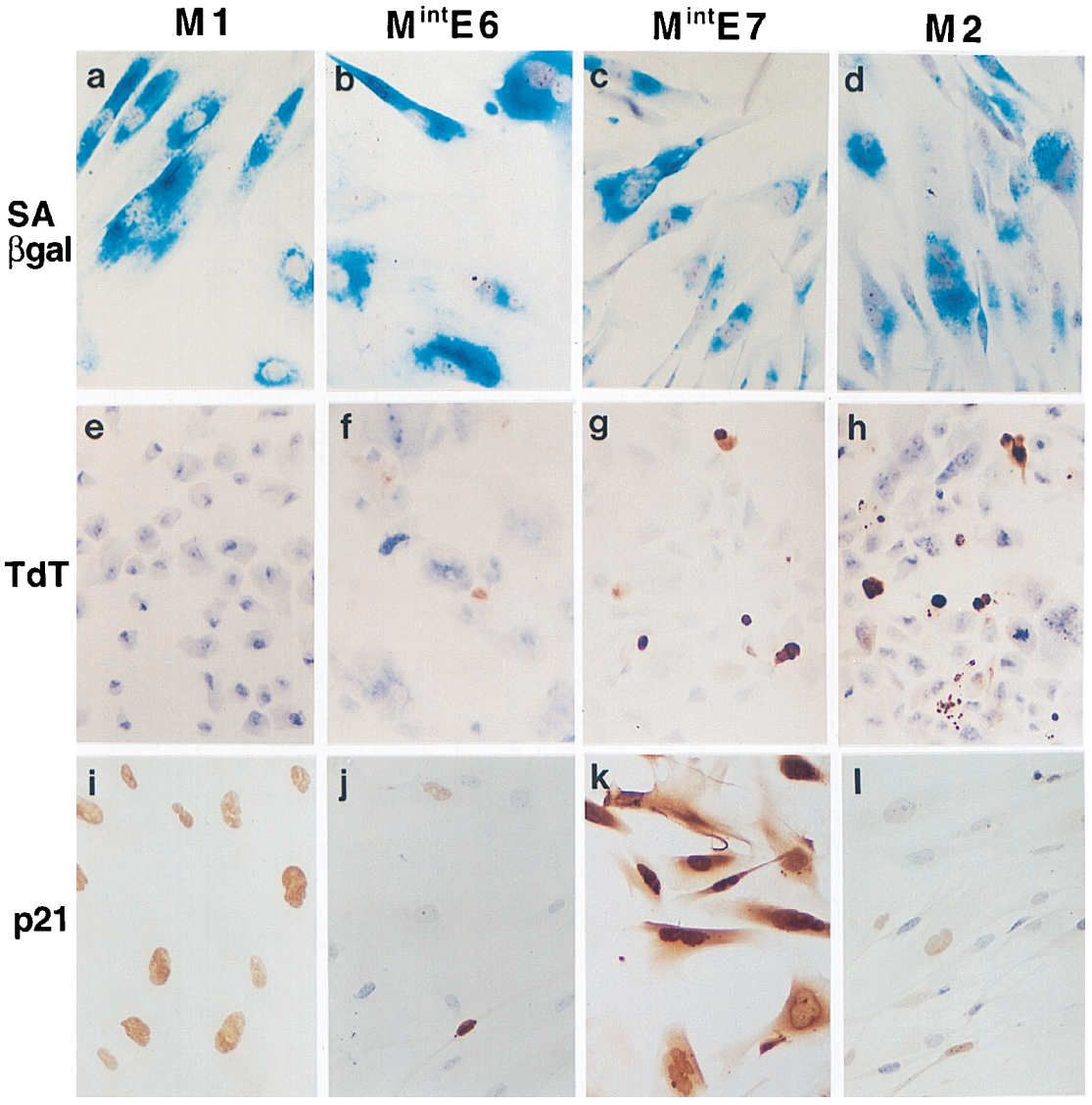

FIG. 2. Further characterization of M^{int} phenotypes in human fibroblasts. (a to d) Histochemical assessment of SAβ-gal activity showing very high expression in M1 (a), $M^{int}E6$ (b), $M^{int}E7$ (c), and M2 (d) growth arrest states. (e to h) TdT assay showing frequent apoptosis in $M^{int}E7$ (g) and M2 (h) states but not at $M^{int}E6$ (f) or M1 (e). (i to l) Immunocytochemical analysis of $p21^{WAF1}$ protein showing further elevation of expression at $M^{int}E7$ (k) above that at M1 (i) contrasting with reduced levels at $M^{int}E6$ (j) and M2 (l). Hematoxylin counterstain; magnification, ×100.

mum of 5×10^{11}. Again, given the presence of cell death, the corresponding values of 31 to 39 PD must be considered underestimates. In summary, therefore, $M^{int}E7$ resembles M2 but occurs sooner and at a much smaller average clone size.

Changes in cell cycle regulators associated with M^{int} states. The above observations allowed us to define a window (Fig. 3) in the growth curves of both HCA2.E6 and E7 cultures corresponding to the point where net growth ceases, referred to here as M^{int}, which was used for all subsequent analyses.

To begin to address the mechanisms of growth arrest, we analyzed the behavior of three cell cycle regulatory proteins—$p21^{WAF1}$, $p16^{INK4a}$, and p53—already known to be involved in control of replicative life span. M1 senescence is associated with increased expression of the CDK inhibitors p21 and p16 (2, 36, 43, 47), and at least for the former there is direct evidence that it plays a necessary role (13). We and others have shown that the increase in p21 in senescent fibroblasts is driven by activation of p53 (23), probably in response to telomere erosion.

$M^{int}E6$ is associated with loss of p21 expression but elevated p16 levels. Intracellular p21 protein content was initially assessed immunocytochemically to permit analysis as soon as possible after introduction of the HPV oncogenes into near-senescent fibroblasts.

Control (HCA2.neo) cells showed high levels of p21 protein in more than 95% of the nuclei (Fig. 2). Introduction of HPVE6 caused a dramatic decrease in both the proportion and intensity of nuclei positive for p21 protein, with <5% of nuclei showing detectable immunostaining at 2 to 3 weeks (data not shown). This was followed by a slow increase in the number, but not the intensity, of immunopositive nuclei, reaching typically 20 to 25% by $M^{int}E6$, although values as low as 10% were observed (Fig. 2).

Western analysis confirmed a reduction in p21 levels in

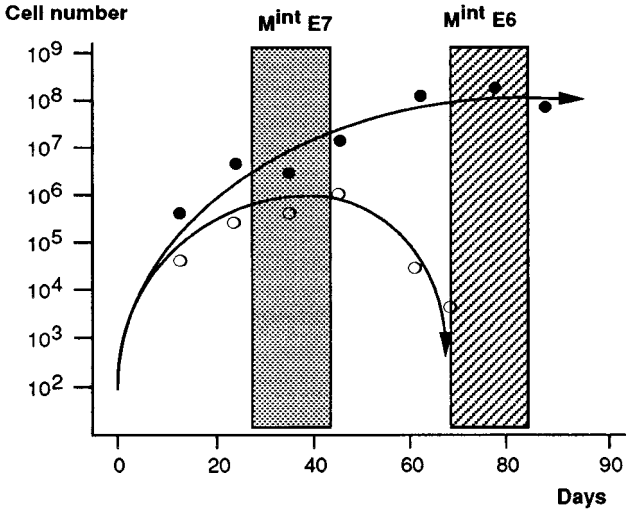

FIG. 3. Contrasting kinetics of growth arrest at $M^{int}E6$ and $M^{int}E7$. Approximately 2×10^5 HDF at <3 PD from senescence were infected with vectors expressing neo plus either HPV E6 (solid symbols) or E7 (open symbols), selected in G418 and maintained in culture with passage as necessary for up to 3 months. Changes in total population size were calculated from passage ratios, and cell counts were performed at the indicated intervals. The initial number of stably infected G418-resistant cells at time 0 was estimated from the colony yield in parallel experiments conducted at clonal density. (No direct cell counts were possible until G418 selection was complete by day 10.) Both E6- and E7-expressing cultures escape senescence and grow for several weeks. With E6, this is followed by a stable state of growth arrest, referred to here as $M^{int}E6$ (hatched zone). In contrast, E7 cultures show only a temporary stationary-growth phase, termed here $M^{int}E7$ (shaded zone), which is followed by progressive net cell loss. These boxed zones of the growth curves define the phases at which cultures were used for all other analyses of the M^{int} phenotypes. Results shown are means of two representative experiments in each case, together with best-fit curves.

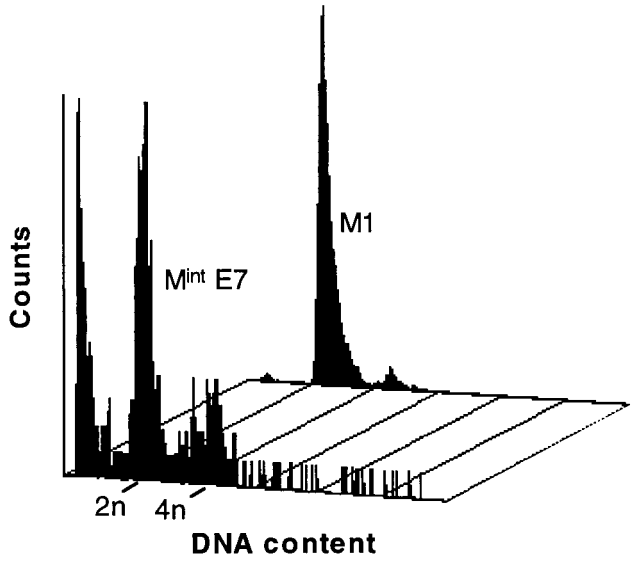

FIG. 4. Flow cytometric analysis of DNA content in human fibroblasts at M1 and $M^{int}E7$. Note prominent sub-G_1 peak in $M^{int}E7$, indicative of apoptosis.

HCA2.E6 cells at $M^{int}E6$ of ~3-fold compared to HCA2.neo at M1 (Fig. 5a). Indeed, when normalized to total protein, to allow for the increased cellular protein content of senescent cells (16), expression at $M^{int}E6$ was comparable to that in young untreated HCA2 fibroblasts (at PD of ~25).

A similar reduction in p21 expression was seen in cultures expressing E6 plus E7 (by both immunocytochemistry and Western analysis). Again, this was followed by a gradual increase, but even at M2 the level remained well below the level seen at M1 (Fig. 2 and 5a).

Immunocytochemical analysis of p16 proved to be unreliable when applied to human fibroblasts due to nonspecific immunostaining visible even in untreated young fibroblasts, having an almost undetectable signal on Western analysis. This unfortunately precluded determination immediately after G418 selection. Nevertheless, at $M^{int}E6$ a reproducible increase in p16 could be demonstrated by Western blotting varying from 2.5- to 3.1-fold over that of control HCA2.neo at M1 (Fig. 5b).

$M^{int}E7$ is associated with increased expression of both p21 and p16. Expression of HPVE7, unlike that of E6, did not lead

TABLE 1. Comparison of M^{int} phenotypes in fibroblasts and thyroid epithelial cells[a]

Indicator	Fibroblasts				Thyrocytes	
	M1 (sen)	$M^{int}E6$ (sen)	$M^{int}E7$ (sen/crisis)	M2 (crisis)	M1[b] (sen)	$M^{int}E7$ (sen/crisis)
Cell kinetics						
Net growth	−	−	−	−	−	−
DNA synthesis	−	−	+	++	−	+
Apoptosis	−	−	+	++	−	+
Senescence marker, SAβ-gal	++	++	++	++	++	++
Cell cycle regulator						
$p21^{WAF1}$	++	+/−	++++	+/−	++	+++
$p16^{INK4a}$	++	+++	+++	++++	−	++

[a] sen, senescence. Values are indicated on a semiquantitative scale from − to ++++.

[b] The term M1 is conserved here for simplicity but does not necessarily imply a common mechanism of terminal growth arrest between normal fibroblasts and thyrocytes.

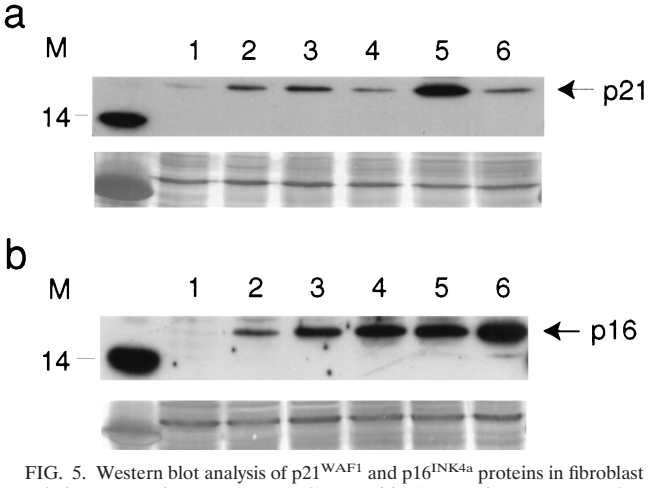

FIG. 5. Western blot analysis of $p21^{WAF1}$ and $p16^{INK4a}$ proteins in fibroblast populations expressing HPV16E6 and/or E7. (a) p21 protein was expressed at higher levels in $M^{int}E7$ cultures (lane 5) and at lower levels in $M^{int}E6$ (lane 4) and M2 (lane 6) cultures compared to a control (neo) M1 population (lane 3). Young cycling fibroblasts at PDL ~25 (lane 1) and uninfected fibroblasts at M1 (lane 2) are shown for comparison. (b) p16 protein was expressed at higher levels in all M^{int} and M2 cultures than at M1. Contents of lanes are the same as those in panel a. Equal amounts (30 μg) of lysate protein were loaded per lane, as verified by India ink staining shown below each blot. Molecular mass markers are shown in kilodaltons.

to a diminution in p21 immunopositivity. On the contrary, as the cells progressed towards $M^{int}E7$, not only did the intensity of positivity increase in virtually all nuclei, but the cytoplasm also became labelled in the majority of cells (Fig. 2). Again, this was confirmed by Western analysis, which showed a four- to sevenfold increase in p21 protein levels in $M^{int}E7$ compared to HCA2.neo (Fig. 5a).

As expected (31), p16 protein was also upregulated by expression of HPVE7, reaching a 2.6- to 4.6-fold increase at $M^{int}E7$ relative to HCA2.neo at M1. An even-greater increase (5.8- to 9.2-fold) was seen in HCA2.E6 plus E7 cells at M2 (Fig. 5a).

Expression of HPVE7 leads to accumulation of nuclear p53 in post-M1 but not in younger fibroblasts. We and others have previously shown that there is no consistent increase in the intracellular content of the p53 protein in human fibroblasts at M1 senescence, despite an increase in both p21 protein levels and p53 transcriptional activity (1, 3, 8, 42). To determine whether this was also true in cells post-M1, immunocytochemical analysis was performed on cells at $M^{int}E6$ and $M^{int}E7$. As before, very little p53 protein was detectable in either young or senescent HCA2.neo (Fig. 6c and e) or $M^{int}E6$ fibroblasts (data not shown). In $M^{int}E7$ cultures, however, there was readily detectable immunopositivity in the majority of nuclei with a marked cell-cell heterogeneity in intensity (Fig. 6f). Importantly, this increase in p53 positivity was not merely a consequence of infection with HPVE7, since young (pre-M1) fibroblasts expressing HPVE7 (Fig. 6d) showed the same barely detectable levels as control HCA2.neo cells at M1, and also cannot be explained by any increase in E7 protein levels in post-M1 compared to pre-M1 cells (Fig. 6a and b).

The increased p53 content at $M^{int}E7$ is associated with increased p53-dependent responses. We have shown previously that blocking p53 function by microinjection of antibodies PAb1801 (5) and DO-1 (44) (both directed at or near the N-terminal transactivation domain of p53) is sufficient to abolish p21 expression in senescent (M1) human fibroblasts (23). The same approach was therefore used to test the p53 dependence of the increase in p21 expression occurring between M1 and $M^{int}E7$.

$M^{int}E7$ cells injected with control IgG displayed very high nuclear and cytoplasmic staining of p21 protein by immunofluorescence analysis in 74.5% ±5% of cells. At 72 h after microinjection with PAb1801, this percentage had fallen to 7.5% ± 1.4%, and the overall level of immunofluorescence was comparable to that observed in actively growing (pre-M1) young fibroblasts (data not shown) and to that in M1 fibroblasts at an identical time after microinjection of PAb1801 (23). A similar reduction in the proportion of p21-positive nuclei, to 8.0% ± 1.4%, was observed following microinjection of DO-1, confirming that, as at M1, the increased expression of p21 at $M^{int}E7$ is p53 dependent.

Table 1 presents a summary of the M^{int} states in comparison to M1 and M2 in human fibroblasts.

Cell type diversity in control of replicative life span: evidence for E7- but not E6-targeted (p53-dependent) senescence pathways in human thyroid epithelial cells. Primary monolayer cultures of follicular cells were prepared from normal human thyroid tissue and infected 2 days later with either control or HPV16-expressing retroviruses. As seen previously (9, 12), cells infected with neo alone stopped proliferating after only 1 to 3 PD and entered a state of prolonged viable quiescence (Fig. 7a). These cultures showed a very low BrdU LI (1 to 3%) and a very high SAβ-gal index (>95%), and high levels of p21 (comparable to those in senescent HDF) were observed in most cells by immunocytochemistry (Fig. 7d and g). On the basis of these criteria they are considered here to be senescent, and for simplicity this state is referred to as M1.

In marked contrast to our results with fibroblasts, but in agreement with previous findings with a dominant-negative mutant p53 (49), infection of primary cultures of near-senescent thyroid epithelial cells with the HPVE6 vector failed to generate any epithelial colonies with an extended life span, indicating that abrogation of p53 function was without effect in these cells. This was confirmed by testing the effect of microinjected anti-p53 antibodies on proliferation and p21 expression in senescent thyrocytes. The BrdU LI 72 h after microinjection did not differ significantly in thyrocytes injected with control IgG, PAb1801, or DO-1 (2% ± 0.2%, 2.5% ± 0.3%, and 2.0% ± 0.2%, respectively). Likewise, the proportion of nuclei containing immunodetectable p21 was not significantly lower than control IgG following PAb1801 or DO-1 injection (Fig. 8). These results indicate that senescence-induced growth arrest and p21 expression are both p53 independent in the normal thyroid cell.

In contrast to infection with HPVE6, infection with HPVE7 generated tight colonies of dividing cells with a typical cobblestone epithelial morphology and nuclei that were much larger than normal (Fig. 7b). When analyzed 6 to 11 weeks after infection, colony size ranged from 1×10^3 to 5×10^5 cells, and BrdU LI reached a maximum of 12 to 17%. Although assessing the percentage of SAβ-gal-positive cells was difficult because of the tightly packed nature of the colonies, levels remained above 50% (Fig. 7e).

$M^{int}E7$ in thyroid epithelial cells shows kinetics similar to that in HDF. Six individual colonies expressing HPVE7 were monitored until net growth ceased, 11 to 20 weeks after infection. By this stage, colonies had become ragged and cells were flattened, with cytoplasmic vacuolation and an increase in both the number and size of the nuclei (Fig. 7c). SAβ-gal positivity was evident in nearly all cells (Fig. 7f). As with HCA2.E7 cultures, growth arrest occurred despite continuing cell proliferation, with the BrdU LI typically remaining at 5 to 6%, and was accompanied by cell death and detachment. The estimated colony cell number at this $M^{int}E7$ stage ranged from 7×10^3 to 1×10^6 cells, representing a minimum of 13 to 20 PD (although again, many individual cells will have undergone considerably more PD).

Infection with HPVE6/E7 produced an outcome similar to that produced by infection with E7, except that colonies showed a less-regular morphology (data not shown) and extended survival time in primary culture. Further follow-up was, however, precluded by the spontaneous development of dedifferentiated subclones following any attempt at passaging, which rapidly became the predominant cell type. This phenomenon was very similar to that observed previously in thyroid epithelial cells expressing SV40 T (12).

$M^{int}E7$ in thyrocytes is associated with increased p16 and p21. As in fibroblasts, M1 thyrocytes at the end of their normal proliferative life span showed readily detectable p21 protein in >95% of nuclei (Fig. 7g). Expression of HPVE7 led initially to a small decrease in the proportion, but not the intensity, of p21-positive nuclei. This, however, returned to 90 to 100% as cultures approached $M^{int}E7$ and was accompanied by an increase in the intensity of nuclear staining as well as the appearance of cytoplasmic positivity as observed in fibroblasts at $M^{int}E7$ (Fig. 7i).

Lack of cell numbers precluded Western analysis of p21 or p16. Fortunately, however, immunocytochemical analysis of p16 when applied to thyroid cells appeared to be free from the

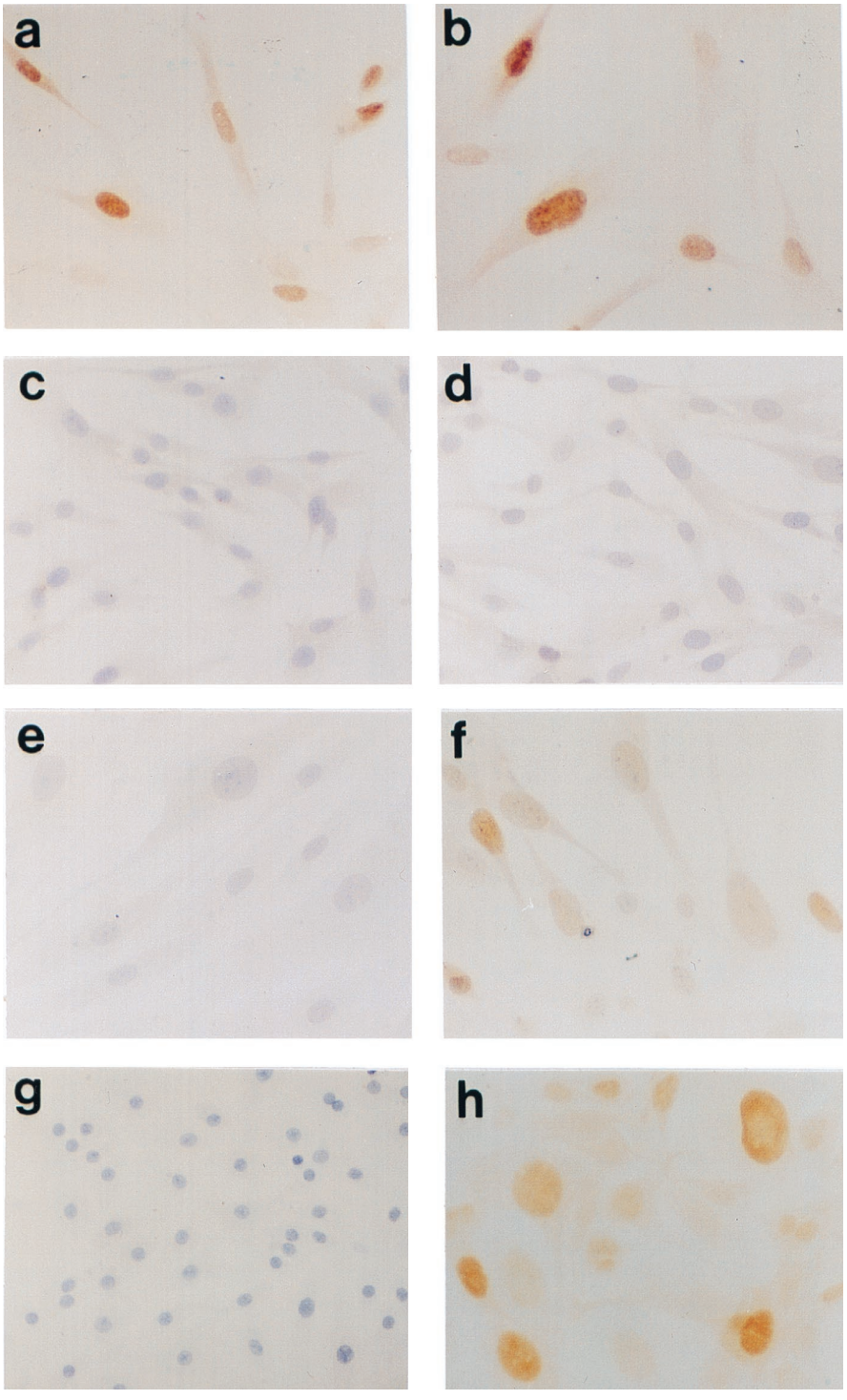

FIG. 6. Increased expression of p53 protein in post-M1 fibroblasts and thyroid epithelial cells expressing HPVE7. Immunocytochemical analysis with PAb421 antibody fails to detect p53 in most young HDF (PDL, ~25), both in neo-only controls (c) and in cells expressing HPVE7 (d). In contrast, readily detectable nuclear p53 with a characteristic cell-cell heterogeneity is seen in HDF expressing E7 at $M^{int}E7$ (f) but not in neo-only cells at M1 (e). These differences in p53 content are not explicable by differences in E7 protein levels, which are similar in both young (a) and post-M1 (b) HDF expressing the E7 vector. A similar heterogeneous elevation of p53 levels is seen in human thyrocytes whose life span has been extended by expression of E7 (h) but not in neo controls at the end of their normal proliferative life span (g). Immunoperoxidase with hematoxylin counterstain; magnification, ×125.

nonspecificity observed with fibroblasts. No immunostaining was detectable in normal thyrocytes before or at M1 (Fig. 7j). However, as HPVE7-induced colonies progressed, cytoplasmic, and to a lesser extent, nuclear positivity developed initially in a patchy distribution but eventually involving the majority of cells at $M^{int}E7$ (Fig. 7l).

$M^{int}E7$ in thyrocytes is associated with increased nuclear p53 content, but expression of p21 is p53 independent. As

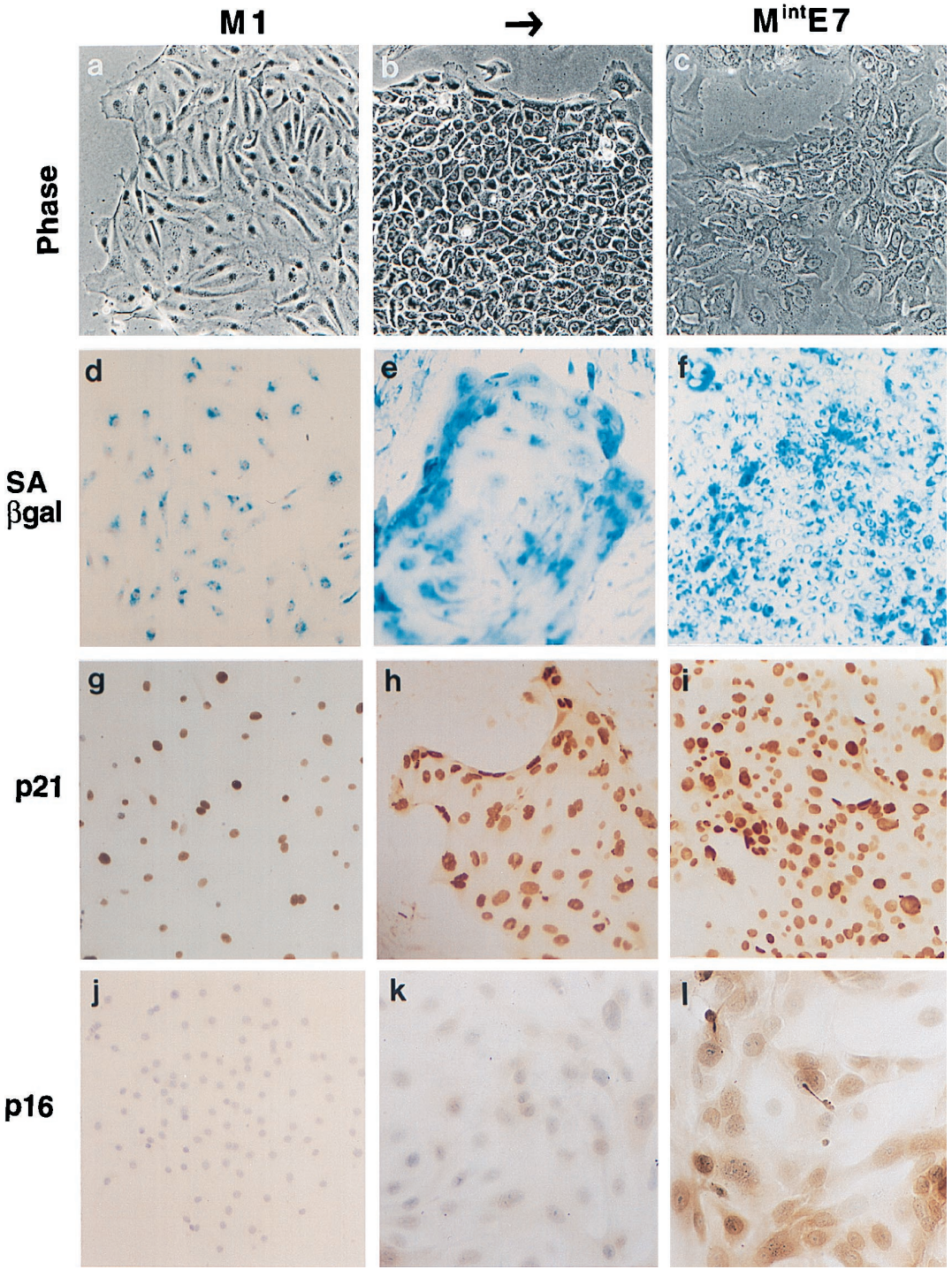

FIG. 7. Phenotypes of human thyroid epithelial cells expressing HPVE7. (a to j) Normal untreated cultures at the end of their normal proliferative life span (M1); (b to k) proliferating colonies induced by expression of HPVE7; (c to l) E7-expressing cultures after net growth has ceased ($M^{int}E7$). All stages show high levels of SAβ-gal (d to f). $p21^{WAF1}$ is readily detectable by immunocytochemistry in most nuclei at M1 (g) and is further induced following extension of life span by E7, even while colonies are still proliferating (h). p16 is undetectable at M1 and in E7-expressing cells is induced later than p21, (l). Note that although terminal growth arrest in normal thyrocytes, or M1, occurs after just a few PD, it may not be triggered by the same underlying regulator as that in HDF. Phase-contrast micrographs (a to c); histochemical β-Gal assay (d to f); immunoperoxidase with hematoxylin counterstain (g to l). Magnification, ×90.

observed in fibroblasts, extension of life span by HPVE7 was associated with a marked increase in nuclear p53 content with the same characteristic cell-cell heterogeneity in intensity of immunostaining (Fig. 6g and h). Due to the limited life span of normal cells, it was not possible to assess the effect of E7 in pre-M1 thyroid cells.

To address whether this increase in p53 content reflected activation of p53, we examined the effect of blocking antibod-

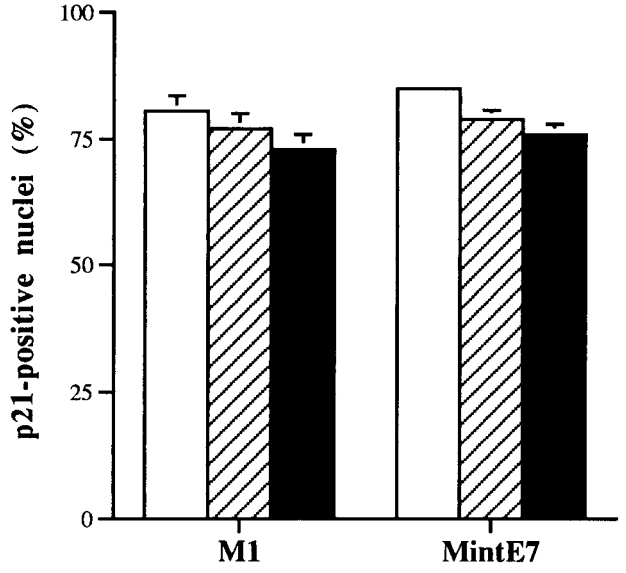

FIG. 8. p53-independent expression of $p21^{waf-1}$ in both normal and HPVE7-expressing thyroid epithelial cells. Thyrocytes at the end of either their normal proliferative lifespan (M1) or the extended life span conferred by HPVE7 ($M^{int}E7$) were microinjected with control IgG (open bars), anti-p53 antibodies PAb1801 (hatched bars), or DO-1 (solid bars). p21 was analyzed 72 h later by immunofluorescence, and the percentage of immunopositive nuclei was counted. Results are shown as means of three replicate experiments ± standard errors of the mean.

ies on the increased expression of p21 at $M^{int}E7$. In sharp contrast to the results obtained in fibroblasts, no effect was seen in thyrocytes. The intensity (data not shown) and proportion of immunopositive nuclei (Fig. 8) after microinjection of PAb1801 or DO-1 (79% ± 1.7% and 76% ± 2%, respectively) were not significantly lower than in control IgG-injected cells (85% ± 1.1%).

Table 1 presents a summary of these data and a comparison with the corresponding phenotypes in fibroblasts.

DISCUSSION

While numerous studies have examined the effects of HPV16E6 and/or E7 on human fibroblasts, few have distinguished between direct actions of the viral genes and indirect effects of life span extension, and to our knowledge none has characterized in detail the eventual fate of these cells.

The detailed kinetic analysis presented here confirms that both genes individually confer an extension of proliferative life span, amounting to approximately half of that achieved by the combination, but reveals in addition a hitherto-unreported distinction between the mechanism of growth arrest in E6 and E7 cultures, the former resulting almost entirely from declining cell birth rate and the latter resulting predominantly from increasing cell death.

Fibroblasts which have evaded senesence (M1) through expression of E6 eventually arrest in a state, termed here $M^{int}E6$, characterized by a return to the very low cell birth rate, high SAβ-gal index, and flat morphology seen at M1. This remarkable similarity of phenotype between $M^{int}E6$ and M1 occurs despite loss of one of the key mediators of M1 senescence, $p21^{WAF1}$, which is undetectable in the majority of cells and reduced overall to a level seen in proliferating pre-M1 cultures. It can be assumed that this results from E6-induced loss of p53, since we have shown by microinjection of anti-p53 antibodies that the elevated level of p21 at M1 is almost entirely p53 dependent (23).

These findings contrast with several recent reports. Filatov et al. (19) found that HDF-expressing E6 ended their proliferative life span in a distinctly different phenotype, with low SAβ-gal and ongoing cell division balanced by death. Furthermore, Brown et al. (13) observed that homozygous disruption of the p21 gene by homologous recombination conferred a prolonged extension of life span, similar to that induced by SV40, and again ending in a state of continuing mitotic activity and death consistent with M2 crisis rather than the $M^{int}E6$ phenotype observed by us. The design of both of these studies, however, involved a much longer period of culture between genetic manipulation of the fibroblasts and eventual growth arrest, hence providing a greater opportunity for acquisition of additional spontaneous changes, such as inactivation of the Rb pathway, which could have prevented an $M^{int}E6$ phenotype becoming manifest. In support of this, observations on LFS fibroblast cultures, in which spontaneous loss of the one remaining wt p53 allele more closely mimics our gene transfer strategy, did reveal a phase of growth arrest consistent with our $M^{int}E6$ phenotype, although this has not been characterized in detail (and in one study [34] was not clearly distinguished from M1).

Our observation that $M^{int}E6$ cells can undergo a stable growth arrest, despite loss of the senescence-associated increase in p21 levels, clearly points to the operation of a compensatory inhibitory pathway (Fig. 9), for which an obvious candidate is p16. In support of this possibility, forced expression of p16 has been shown to be able to restore growth arrest in both young (33) and immortalized (43) human fibroblasts. Furthermore, rare spontaneous escape from the equivalent state to $M^{int}E6$ in LFS fibroblasts is associated with loss of p16 expression (39). We have indeed shown that this CDK inhibitor is further induced by ~3-fold at $M^{int}E6$ compared to M1, which may reinstate the level of CDK inhibition required for growth arrest, and consistent with this, preliminary analysis (data not shown) indicates that the pRb protein at $M^{int}E6$ is predominantly in the unphosphorylated form. We cannot at this stage, however, exclude the possibility that while the elevation of p16 is probably necessary, it may not be sufficient for $M^{int}E6$ (Fig. 9b). To investigate further the existence of an additional pathway(s), we are currently analyzing the levels of p16 and other CDK inhibitors, as well as the activity of cyclin-CDK complexes, throughout the M1 to $M^{int}E6$ interval. We have also begun a parallel study with fibroblasts containing a homozygous germ line intragenic deletion in p16 (24, 37a) to determine if these cells will also be capable of entering a stable growth arrest state equivalent to $M^{int}E6$ when expressing HPVE6.

In sharp contrast to $M^{int}E6$, the corresponding state in fibroblasts expressing E7, while associated with some diminution in DNA synthesis, results predominantly from an increase in cell death rate, much if not all of which appears apoptotic in nature. It therefore resembles the typical crisis state (M2) seen in cells expressing E6 and E7 but occurring after a much shorter period of life span extension and at a much smaller clone size. We have shown that this process is associated with a marked increase in nuclear p53 content and a corresponding p53-dependent increase in p21 expression over and above the elevation already present at M1. These changes in p53 status were notably absent in young (pre-M1) fibroblasts expressing E7, demonstrating that they depend on the extension of life span resulting from E7 rather than being simply a direct effect of cell cycle dysregulation by E7. Although evidence for similar behavior can be seen in other cell types, e.g., breast epithelial

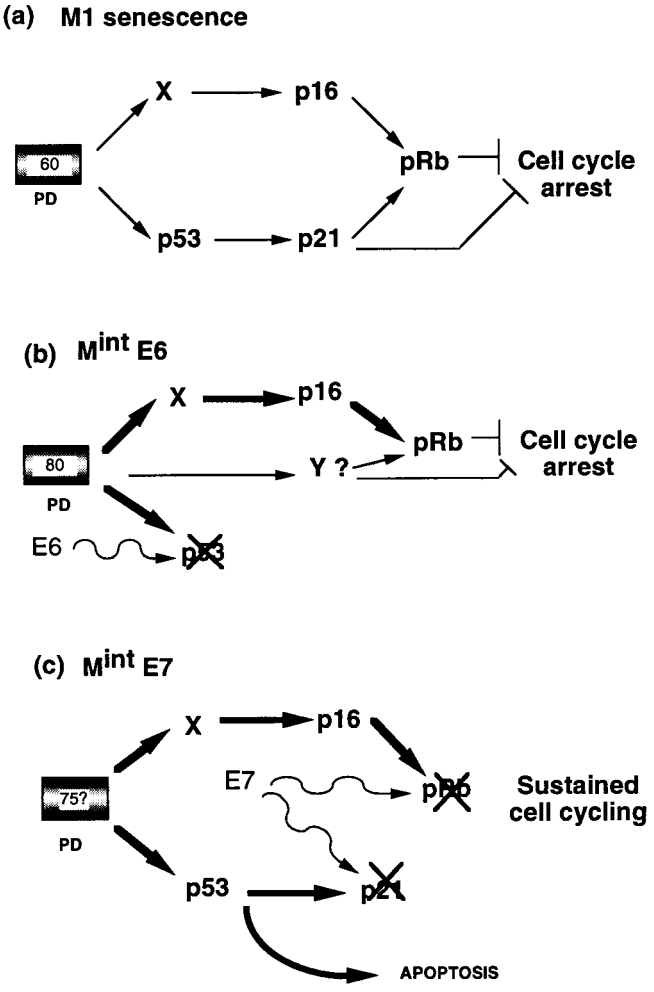

FIG. 9. Models to explain M^{int} growth arrest states in human fibroblasts. (a) Normal senescence (M1) is assumed to be mediated by at least two signal pathways activated by a cell-cycle clock after around 60 PD (now almost certainly linked to telomere erosion). Both of these converge to inhibit phosphorylation of Rb by CDKs. p21 may also inhibit cell cycle progression via other targets (51). (b) $M^{int}E6$. Cells which have initially escaped senescence by E6-mediated loss of the p53 pathway are able to reestablish cell cycle arrest approximately 20 PD later. One mechanism is further upregulation of the p16 pathway, which may compensate for the loss of p21, although our data do not exclude the requirement for an additional, as-yet-unknown, pathway(s) indicated by Y. (c) $M^{int}E7$. Escape from senescence induced by HPVE7 is associated with a more profound disruption of cell cycle control through abrogation of pRb and p21 (22, 30a), which prevents restoration of cell cycle arrest. Clonal expansion is finally limited by apoptosis mediated at least in part by p53.

cells (20) and keratinocytes (17), the importance of proliferative age has not been emphasized in previous studies, most of which have analyzed effects of E7 on p53 function in cell lines (28, 38).

Recent evidence suggests that release of E2F following abrogation of Rb function by E7 can activate transcription of the alternative product of the $p16^{INK4a}$ locus $p14^{ARF}$ (6). This in turn has been shown to neutralize the effect of mdm2, resulting in stabilization and activation of p53. Such a pathway is not, however, sufficient to explain why p53 content should be elevated only in cells which have passed M1 and not at or before M1. (We have excluded the possibility of an increased expression of E7 post-M1.) It appears therefore that increasing replicative age leads to the generation of additional and/or more intense p53-modifying signals, most obviously as a result of further telomere erosion (19). There is an interesting precedent for this (29) in the response to DNA damage by UV irradiation in which low doses result in activation of p53 without stabilization (equivalent to M1 here), followed by stabilization at higher doses (analogous to $M^{int}E7$).

These changes in p53 activity are likely to contribute to the increasing cell death at $M^{int}E7$ (Fig. 9c). Although microinjection studies in these apoptotic cultures have proven difficult to interpret, a role for p53 can be inferred from the absence of cell death at the corresponding stage in development of cultures expressing E6 in addition to E7. We also have preliminary evidence that sequential gene transfer of E6- into E7-expressing cells close to $M^{int}E7$ results in rescue from cell death, consistent with loss of p53 function.

The failure of $M^{int}E7$ cells to undergo p53-mediated growth arrest is probably due to abrogation not only of Rb but also of $p21^{WAF1}$ function by HPVE7 (Fig. 9c). E7 has been demonstrated to bind to p21 and block both its CDK- and PCNA-inhibitory actions, both in intact cells and in cell-free systems (22, 30a), a viral function which probably evolved (22) to prevent inhibition of DNA replication by p21 via targets other than Rb (e.g., E2F or PCNA).

Currently, a popular explanation for the existence of multiple genetic abnormalities in cancer cells is that single events often lead to compensatory inhibitory effects which require a second gene mutation for their avoidance. A classic paradigm for this is the cooperation between Rb and p53 mutation which several experimental models have suggested is based on the need to overcome an immediate p53-induced cell death response triggered by loss of Rb function (35, 37). Our study illustrates a different model in which the basis of tumor suppressor gene cooperation is seen as the need to escape successive proliferative life span barriers. The essential conceptual difference is that in this case the mutations can occur sequentially rather than concurrently. This is a much more likely scenario, since the period of proliferation afforded by the first mutation generates a large population of potential target cells before the second mutation becomes necessary.

Our data also demonstrate how the nature and timing of these PLBs can differ markedly between different cell types. Thyroid epithelial cells, for example, undergo a terminal arrest state closely resembling classic M1 senescence (in terms of cell kinetics, morphology, SAβ-gal, and p21 expression) but occurring after a remarkably small number of PD (12). We are confident that this is not merely an artifact of adverse tissue culture conditions, since a similar limitation of life span is observed when thyroid cells are stimulated to proliferate in the intact tissue by their physiological mitogen, thyrotropin (9, 50). Furthermore, thyroid cells are capable of rapid proliferation for a much longer number of PD in the same culture conditions if provided with a more powerful growth stimulus, such as that generated by a mutant *ras* gene (9).

At present we do not know how this precocious senescence is triggered in thyroid cells, but as with a similar phenomenon recently reported in fibroblasts (40), it is highly unlikely to be regulated by a telomere-based system. Indeed, preliminary analysis (30) suggests that thyroid cells senesce with mean telomere lengths at least 2 kb above those of senescent fibroblasts. The important feature revealed here, though, is that unlike both the classic M1 senescence and the recently described premature senescent states in fibroblasts, in thyrocytes growth arrest does not appear to involve a p53-dependent pathway. This is clearly shown by the failure of E6 to extend life span and by failure of p53-blocking antibodies to stimulate DNA synthesis. It is also consistent with our finding that the

high level of p21 in these cells is driven by a p53-independent mechanism whose nature is currently under investigation.

The existence of an early senescent state in thyrocytes which can be overcome by expression of E7 but not E6 is reminiscent of a similar state termed M0 in human breast epithelial cells (20, 21). In both cell types, however, E7 confers only a limited extension of life span, leading eventually to a second arrest state, referred to here as $M^{int}E7$. The kinetics of this are similar to the corresponding state in fibroblasts, being predominantly due to cell death but occurring over a more protracted time scale. As in the fibroblast, this is associated with a marked elevation of nuclear p53 content, but it has as yet proven difficult to determine whether this plays any casual role, since comparison with thyroid cells expressing both E6 and E7 is vitiated by the high frequency of spontaneous dedifferentiation found in these cultures, similar to that observed previously with SV40 (12).

These cell type differences observed in vitro are intriguingly consistent with the results of genetic analysis of clinical tumor samples. These have shown that in contrast to the majority of human cancers, including those of fibroblast origin, differentiated thyroid and most breast cancers exhibit a very low prevalence of p53 mutation (50, 52). We suggest, therefore, that the nature of the genes regulating PLBs in a given cell type may determine the selection pressure for mutation and hence the pattern of tumor suppressor gene inactivation observed in the corresponding tumors.

ACKNOWLEDGMENTS

We thank James Smith (Houston), Denise Galloway (Seattle), David Lane (Dundee) and Jiri Bartek (Danish Cancer Society) for kind gifts of cells, retrovirus vectors, and antibodies, and Roger Reddel (Sydney) and Gordon Peters (ICRF, London) for valuable advice and comments. We are grateful to Theresa King for manuscript preparation.

We are grateful to the Cancer Research Campaign and the Medical Research Council for grant support.

REFERENCES

1. **Afshari, C. A., P. J. Vojta, L. A. Annab, P. A. Futreal, T. B. Willard, and J. C. Barrett.** 1993. Investigation of the role of G1/S cell cycle mediators in cellular senescence. Exp. Cell Res. **209:**231–237.
2. **Alcorta, D. A., Y. Xiong, D. Phelps, G. Hannon, D. Beach, and J. C. Barrett.** 1996. Involvement of the cyclin-dependent kinase inhibitor p16 (INK4a) in replicative senescence of normal human fibroblasts. Proc. Natl. Acad. Sci. USA **93:**13742–13747.
3. **Atadja, P., H. Wong, I. Garkavtsev, C. Geillette, and K. Riabowol.** 1995. Increased activity of p53 in senescing fibroblasts. Proc. Natl. Acad. Sci. USA **92:**8348–8352.
4. **Bacchetti, S.** 1996. Telomere dynamics and telomerase activity in cell senescence and cancer. Cell Dev. Biol. **7:**31–39.
5. **Banks, L., G. Matlashewski, and L. Crawford.** 1986. Isolation of human p53 specific monoclonal antibodies and their use in the study of human p53 expression. Eur. J. Biochem. **159:**529–534.
6. **Bates, S., A. C. Phillips, P. A. Clark, F. Stott, G. Peters, R. L. Ludwig, and K. H. Vousden.** 1998. $p14^{ARF}$ links the tumor suppressors Rb and p53. Nature **395:**124–125.
7. **Bond, J., T. Dawson, N. R. Lemoine, and D. Wynford-Thomas.** 1992. Effect of serum growth factors and phorbol ester on growth and survival of human thyroid epithelial cells expressing mutant ras. Mol. Carcinog. **5:**129–135.
8. **Bond, J., M. Haughton, J. Blaydes, V. Gire, D. Wynford-Thomas, and F. Wyllie.** 1996. Evidence that transcriptional activation by p53 plays a direct role in the induction of cellular senescence. Oncogene **13:**2097–2104.
9. **Bond, J. A., F. S. Wyllie, J. Rowson, A. Radulescu, and D. Wynford-Thomas.** 1994. In vitro reconstruction of tumour initiation in a human epithelium. Oncogene **9:**281–290.
10. **Bond, J. A., J. P. Blaydes, J. Rowson, M. F. Haughton, J. R. Smith, D. Wynford-Thomas, and F. S. Wyllie.** 1995. Mutant p53 rescues human diploid cells from senescence without inhibiting the induction of SD11/WAF1. Cancer Res. **55:**2404–2409.
11. **Bond, J. A., F. S. Wyllie, and D. Wynford-Thomas.** 1994. Escape from senescence in human diploid fibroblasts induced directly by mutant p53. Oncogene **9:**1885–1889.
12. **Bond, J. A., G. O. Ness, J. Rowson, M. Ivan, D. White, and D. Wynford-Thomas.** 1996. Spontaneous de-differentiation correlates with extended lifespan in transformed thyroid epithelial cells: an epigenetic mechanism of tumour progression. Int. J. Cancer **67:**563–572.
13. **Brown, J. P., W. Wenyi, and J. M. Sedivy.** 1997. Bypass of senescence after disruption of p21CIP1/WAF1 gene in normal diploid human fibroblasts. Science **277:**831–834.
14. **Bryan, T. M., and R. R. Reddel.** 1994. SV40-induced immortalization of human cells. Crit. Rev. Oncog. **5:**331–357.
15. **Bryan, T. M., A. Englezou, J. Gupta, S. Bacchetti, and R. R. Reddel.** 1995. Telomere elongation in immortal human cells without detectable telomerase activity. EMBO J. **14:**4240–4248.
16. **Cristofalo, V. J., and R. J. Pignolo.** 1993. Replicative senescence of human fibroblast-like cells in culture. Physiol. Rev. **73:**617–638.
17. **Demers, G. W., C. L. Halbert, and D. A. Galloway.** 1994. Elevated wild-type p53 protein levels in human epithelial cell lines immortalized by the human papillomavirus type 16 E7 gene. Virology **198:**169–174.
18. **Dimri, G. P., X. Lee, G. Basile, M. Acosta, G. Scott, C. Roskelley, E. E. Medrano, M. Linskens, I. Rubelj, O. Pereira-Smith, M. Peacocke, and J. Campisi.** 1995. A biomarker that identifies senescent human cells in culture and in aging skin in vivo. Proc. Natl. Acad. Sci. USA **92:**9363–9367.
19. **Filatov, L., V. Golubovskaya, J. C. Hurt, L. L. Byrd, J. M. Phillips, and W. K. Kaufmann.** 1998. Chromosomal instability is correlated with telomere erosion and inactivation of G2 checkpoint function in human fibroblasts expressing human papillomavirus type 16 E6 oncoprotein. Oncogene **16:**1825–1838.
20. **Foster, S. A., and D. A. Galloway.** 1996. Human papillomavirus type 16 E7 alleviates a proliferation block in early passage human mammary epithelial cells. Oncogene **12:**1773–1779.
21. **Foster, S. A., D. J. Wong, M. T. Barrett, and D. A. Galloway.** 1998. Inactivation of p16 in human mammary epithelial cells by CpG island methylation. Mol. Cell. Biol. **18:**1793–1801.
22. **Funk, J. O., S. Waga, J. B. Harry, E. Espling, B. Stillman, and D. A. Galloway.** 1997. Inhibition of CDK activity and PCNA-dependent DNA replication by p21 is blocked by interaction with the HPV-16 E7 oncoprotein. Genes Dev. **11:**2090–2100.
23. **Gire, V., and D. Wynford-Thomas.** 1998. Reinitiation of DNA synthesis and cell division in senescent human fibroblasts by microinjection of anti-p53 antibodies. Mol. Cell. Biol. **18:**1611–1621.
24. **Gruis, N. A., P. A. van der Velden, K. A. Sandkuijl, D. E. Prins, J. Weaver-Feldhaus, A. Kamb, W. Bergman, and R. R. Frants.** 1995. Homozygotes for CDKN2 (p16) germline mutation in Dutch familial melanoma kindreds. Nat. Genet. **10:**351–353.
25. **Halbert, C. L., G. W. Demers, and D. A. Galloway.** 1991. The E7 gene of human papillomavirus type 16 is sufficient for immortalization of human epithelial cells. J. Virol. **65:**473–478.
26. **Harlow, E., L. V. Crawford, D. C. Pim, and N. M. Williamson.** 1981. Monoclonal antibodies specific for simian virus 40 tumor antigens. J. Virol. **39:**861–869.
27. **Hayflick, L.** 1965. The limited in vitro lifetime of human diploid cell strains. Exp. Cell Res. **37:**614–636.
28. **Hickman, E. S., S. Bates, and K. H. Vousden.** 1997. Perturbation of the p53 response by human papillomavirus type 16 E7. J. Virol. **71:**3710–3718.
29. **Hupp, T. R., A. Sparks, and D. P. Lane.** 1995. Small peptides activate the latent sequence-specific DNA binding function of p53. Cell **83:**237–245
30. **Jones, C. J., and D. Wynford-Thomas.** Unpublished data.
30a. **Jones, D. L., R. M. Alani, and K. Munger.** 1997. The human papillomavirus E7 oncoprotein can uncouple cellular differentiation and proliferation in human keratinocytes by abrogating $p21^{Cip-1}$-mediated inhibition of cdk2. Genes Dev. **11:**2101–2111.
31. **Li, Y., M. A. Nichols, J. W. Shay, and Y. Xiong.** 1994. Transcriptional repression of the D-type cyclin-dependent kinase inhibitor p16 by the retinoblastoma susceptibility gene product, pRb. Cancer Res. **54:**6078–6082.
32. **Lukas, J., D. Parry, L. Aagaard, D. J. Mann, J. Bartkova, M. Strauss, G. Peters, and J. Bartek.** 1995. Retinoblastoma-protein-dependent cell-cycle inhibition by the tumor suppressor p16. Nature **375:**503–506.
33. **McConnell, B. B., M. Starborg, S. Brookes, and G. Peters.** 1998. Inhibitors of cyclin-dependent kinases induce features of replicative senescence in early passage human diploid fibroblasts. Curr. Biol. **8:**351–354.
34. **Medcalf, A. S. C., A. J. P. Klein-Szanto, and V. J. Cristofalo.** 1996. Expression of p21 is not required for senescence of human fibroblasts. Cancer Res. **56:**4582–4585.
35. **Morgenbesser, S. D., B. O. Williams, T. Jacks, and R. A. dePinho.** 1994. p53-dependent apoptosis produced by Rb-deficiency in the developing mouse lens. Nature **371:**72–74.
36. **Noda, A., Y. Ning, S. F. Venable, O. M. Pereira-Smith, and J. R. Smith.** 1994. Cloning of senescent cell-derived inhibitors of DNA synthesis using an expression screen. Exp. Cell Res. **211:**90–98.
37. **Pan, H., and A. E. Griep.** 1994. Altered cell cycle regulation in the lens of HPV-16 E6 or E7 transgenic mice: implications for tumour suppressor gene function in development. Genes Dev **8:**1285–1299.
37a. **Peters, G.** Personal communication.

38. **Puthenveettil, J. A., S. M. Frederickson, and C. A. Reznikoff.** 1996. Apoptosis in human papillomavirus 16 E7-, but not E6-immortalized human uroepithelial cells. Oncogene **13:**1123–1131.
39. **Rogan, E. M., T. M. Bryan, B. Hukku, K. Maclean, A. C.-M. Chang, E. L. Moy, A. Englezou, S. G. Warneford, L. Dalla-Pozza, and R. R. Reddel.** 1995. Alterations in p53 and $p16^{INK4}$ expression and telomere length during spontaneous immortalization of Li-Fraumeni syndrome fibroblasts. Mol. Cell. Biol. **15:**4745–4753.
40. **Serrano, M., A. W. Lin, M. E. McCurrach, D. Beach, and S. W. Lowe.** 1997. Oncogenic ras provokes premature cell senescence associated with accumulation of p53 and p16INK4a. Cell **88:**593–602.
41. **Shay, J. W., W. E. Wright, D. Brasiskyte, and B. A. Van der Hagen.** 1993. E6 of human papillomavirus type 16 can overcome the M1 stage of immortalisation in human mammary epithelial cells but not human fibroblasts. Oncogene **8:**1407–1413.
42. **Vaziri, H., M. D. West, R. C. Allsopp, T. S. Davison, Y.-S. Wu, C. H. Arrowsmith, G. G. Poirier, and S. Benchimol.** 1997. ATM-dependent telomere loss in aging human diploid fibroblasts and DNA damage lead to the post-translational activation of p53 protein involving poly (ADP-ribose) polymerase. EMBO J. **16:**6018–6033.
43. **Vogt, M., C. Haggblom, J. Yeargin, T. Christiansen-Weber, and M. Haas.** 1998. Independent induction of senescence by p16INK4a and p21CIP1 in spontaneously immortalized human fibroblasts. Cell Growth Differ. **9:**139–146.
44. **Vojtesek, B., J. Bartek, C. A. Midgley, and D. P. Lane.** 1992. An immunochemical analysis of the human nuclear phosphoprotein p53. J. Immunol. Methods **151:**237–244.
45. **White, A. E., E. M. Livanos, and T. D. Tlsty.** 1994. Differential disruption of genomic integrity and cell cycle regulation in normal human fibroblasts by the HPV oncoproteins. Genes Dev **8:**666–677.
46. **Williams, D. W., E. D. Williams, and D. Wynford-Thomas.** 1988. Loss of dependence in IGF-1 for proliferation of human thyroid adenoma cells. Br. J. Cancer **57:**535–539.
47. **Wong, H., and K. Riabowol.** 1996. Differential cdk-inhibitor gene expression in aging human diploid fibroblasts. Exp. Gerontol. **31:**311–325.
48. **Wright, W. E., O. M. Pereira-Smith, and J. W. Shay.** 1989. Reversible cellular senescence: implications for immortalization of normal human diploid fibroblasts. Mol. Cell. Biol. **9:**3088–3092.
49. **Wyllie, F., N. Lemoine, C. Barton, T. Dawson, J. Bond, and D. Wynford-Thomas.** 1993. Direct growth stimulation of normal human epithelial cells by mutant p53. Mol. Carcinogen **7:**83–88.
50. **Wynford-Thomas, D.** 1995. Molecular genetics of thyroid cancer. Curr. Opin. Endocr. Diabetes **2:**429–436.
51. **Wynford-Thomas, D.** 1997. Proliferative lifespan checkpoints: cell-type specificity and influence on tumour biology. Eur. J. Cancer **33:**716–726.
52. **Wynford-Thomas, D., and J. P. Blaydes.** 1998. The influence of cell context on the selection pressure for p53 mutation in human cancer. Carcinogen **19:**29–36.